Inversion = migration + tomography

Peter Mora
Thinking Machines Corporation 245 First St. Cambridge, MA, 02142

ABSTRACT

Seismic inversion, broadly enough defined, is equivalent to doing migration and reflection tomography simultaneously. Diffraction tomography and inversion work best when sources and receivers surround the region of interest, as in medical imaging applications. Theoretical studies typically show that the high vertical wavenumber velocity perturbations are resolved in seismic reflection experiments where the sources and receivers are restricted to the Earth's surface but low vertical wavenumbers must be obtained using a separate step such as a velocity analysis or reflection tomography. I propose that an iterative inversion using a *varying background velocity obtains all wavenumbers* that are resolvable separately by migration and tomography. (The background velocity must contain *abrupt* discontinuities.) Reflectors in the background model simulate sources and receivers within the Earth so the source and receiver coverage in seismic reflection inverse problems is effectively the same as in medical imaging. Some synthetic examples verify the theoretical predictions and show that reflector locations and interval velocities can be obtained simultaneously.

INTRODUCTION

Typical analyses of the seismic inverse problem with sources and geophones on the Earth's surface indicate that the velocity image will only be partially reconstructed (Devaney, 1984; Devaney and Beylkin, 1984; Esmersoy et al., 1985; Esmersoy and Levy, 1986; Wu and Toksöz, 1987). Even when source-geophone offsets extend from zero to infinity, only the high vertical wavenumbers are resolved and inversion results look like migration

results and do not resolve, but rather require, a smooth (low-wavenumber) velocity model (Mora, 1987b).

This is strange considering that inversion purports to obtain a velocity model from which synthetic data could be generated that best matches the observed seismic wavefield. It is well known that shapes of reflection hyperbolas can be used to obtain the low-wavenumber velocity model, so the low-wavenumber information *is* contained in the seismic wavefield. However, it is hard to extract this low-wavenumber information unless some assumptions about the shape of reflectors are made. For instance, velocity analysis typically assumes flat reflectors (and small incidence angles) and tomography often makes assumptions about the reflectors (for example that the reflectors have been identified or that reflectors are flat or continuous). However, an inversion that best matches the observed seismic wavefield to a synthetic wavefield should obtain all resolvable wavenumber components in a velocity model. In order to account for the shapes of reflection hyperbolas, the low-wavenumber velocity model must be correct. To account for reflection amplitudes the high-wavenumber velocity model must be correct. What is the problem with the analyses that indicate that these low wavenumbers cannot be obtained? Or is it a problem in the inversion algorithms themselves?

An analysis using a *non-constant* background model containing a deep reflecting interface indicates that *all* wavenumbers can be resolved up to some maximum value for the case when offset extends from zero to infinity. This value depends on the maximum frequency in the seismic wavelet. Therefore, provided the inversion assumes a background model that is *non-constant* and contains the reflector locations, the inversion is capable of resolving all wavenumbers. Considering the first iteration of an iterative inversion approximately locates the reflectors, it is not really necessary to know the reflector locations a priori. Consequently, an *iterative* inversion that allows both the *high- and low-wavenumber components of the background model to vary* is a *complete* inversion. In other words, it resolves both reflector locations as well as interval velocities simultaneously.

NON-CONSTANT BACKGROUND SCATTERING AND INVERSION

I will assume the simplest wave equation, the acoustic wave equation, to simplify algebra. This enables the reader to focus on the main problem of obtaining high- and low-wavenumber velocity models simultaneously. Of course, all the concepts apply equally well to the full anisotropic elastic wave equation. A future paper will detail these extensions.

To explore which part of the wavenumber spectrum can be obtained in an inversion, consider first the basic plane wave experiment in Figure 1. A plane wave is incident on some anomalous region and both the sources and the geophones are located along a horizontal line which is assumed to be far from the velocity anomaly (the source/geophone line would normally be the Earth's surface). A simple non-constant background velocity is assumed, namely two homogeneous halfspaces or equivalently, a layer over a halfspace with an absorbing boundary condition at the Earth's surface. Note that I use an absorbing rather than a more realistic free surface boundary condition to simplify the mathematical development. Usage of an absorbing boundary condition will not affect from my conclusions because they are based on first order effects whereas multiple reflections generated by a free surface are of second order. Hence, within the context of this paper, I use the term "source/geophone surface" interchangeability with "Earth's surface". It is the reflection from the halfspace-halfspace interface that enables the low wavenumbers in the velocity anomaly to be resolved in an inversion. (This reflection event helps to resolve the "interval velocities" in the region between the interface and the Earth's surface.) This is comparable to the case of reflection tomography but, as we will see in the example, locations of reflectors can be determined by the inversion and are therefore not required a priori.

The following is a derivation of the scattering formulas which relate the scattered field to the spectrum of the velocity anomaly (see Wu and Toksöz (1987) for the equivalent constant background velocity derivation).

For monochromatic waves, the constant-density acoustic wave equation is

$$\nabla^2 u(\underset{\sim}{r}_s,\underset{\sim}{r}) + \omega^2 W(\underset{\sim}{r}_s,\underset{\sim}{r}) u(\underset{\sim}{r}_s,\underset{\sim}{r}) = f(\underset{\sim}{r}_s) \quad , \tag{1}$$

where $u(\underset{\sim}{r}_s,\underset{\sim}{r})$ is the scalar quantity of the wavefield at position $\underset{\sim}{r}$ (such as the pressure), ω is the angular frequency, $f(\underset{\sim}{r}_s)$ is the source function at frequency ω, $\underset{\sim}{r}_s$ is the source position, and $W(\underset{\sim}{r})$ is the squared slowness (i.e. $W(\underset{\sim}{r}) = 1/v^2(\underset{\sim}{r})$ where $v(\underset{\sim}{r})$ is the velocity of acoustic wave propagation).

In the following development, I will apply the wave equation and first order Born approximation to obtain an expression for the perturbation in the wavefield δu in terms of the perturbation in the squared slowness δW. I will then specialize this result to a particular non-constant background, namely a two-halfspace model. Restricting the region of interest to be the upper halfspace and using the formula for δu, I will derive the inverse formula for δW in terms of δu in the Fourier domain. This inverse formula for the squared slowness in

the wavenumber domain is the main result of this paper and will be interpreted with the help of Figures and numerical examples.

Defining the squared slowness field to be a constant background $W_0(\underset{\sim}{x}) = 1/v_0^2(\underset{\sim}{x})$ plus some relative perturbation denoted $\delta W(\underset{\sim}{x})$,

$$W(\underset{\sim}{x}) = W_0(\underset{\sim}{x})[1 + \delta W(\underset{\sim}{x})] \quad , \tag{2}$$

and defining the wavenumber $k = k(\underset{\sim}{x}) = \omega/v_0(\underset{\sim}{x})$ we obtain

$$\nabla^2 u(\underset{\sim}{x}_s,\underset{\sim}{x}) + k^2 u(\underset{\sim}{x}_s,\underset{\sim}{x}) = -k^2 \delta W(\underset{\sim}{x}) u(\underset{\sim}{x}_s,\underset{\sim}{x}) + f(\underset{\sim}{x}_s) \quad . \tag{3}$$

Now, by defining the wavefield $u(\underset{\sim}{x}_s,\underset{\sim}{x})$ in terms of the wavefield in the unperturbed medium $u_0(\underset{\sim}{x}_s,\underset{\sim}{x})$ as

$$u(\underset{\sim}{x}_s,\underset{\sim}{x}) = u_0(\underset{\sim}{x}_s,\underset{\sim}{x}) + \delta u(\underset{\sim}{x}_s,\underset{\sim}{x}) \quad , \tag{4}$$

and applying the first order Born approximation, namely that higher order terms of form $O^2(\delta u, \delta W)$ can be neglected, and applying equation (1) yields

$$\nabla^2 \delta u(\underset{\sim}{x}_s,\underset{\sim}{x}) + k^2 \delta u(\underset{\sim}{x}_s,\underset{\sim}{x}) = -k^2 \delta W(\underset{\sim}{x}) u_0(\underset{\sim}{x}_s,\underset{\sim}{x}) \quad . \tag{5}$$

The solution to this equation in terms of the acoustic wave equation Green's functions for the medium $G(\underset{\sim}{x}',\underset{\sim}{x})$ is

$$\begin{aligned} \delta u(\underset{\sim}{x}_s,\underset{\sim}{x}) &= \int_V k^2 \delta W(\underset{\sim}{x}') u_0(\underset{\sim}{x}_s,\underset{\sim}{x}') G(\underset{\sim}{x}',\underset{\sim}{x}) d\underset{\sim}{x}' \\ &= \int_V k^2 \delta W(\underset{\sim}{x}') G(\underset{\sim}{x}_s,\underset{\sim}{x}') f(\underset{\sim}{x}_s) G(\underset{\sim}{x}',\underset{\sim}{x}) d\underset{\sim}{x}' \quad . \end{aligned} \tag{6}$$

So far the discussion has been valid for sources located without restriction at $\underset{\sim}{x}_s$ and geophones at $\underset{\sim}{x}$. Now, restricting the sources and geophones to be located on the Earth's surface yields

$$\delta u(x_s, x_g) = \int_V k^2 \delta W(\underset{\sim}{x}) G(x_s,\underset{\sim}{x}) f(x_s) G(x_g,\underset{\sim}{x}) d\underset{\sim}{x} \quad . \tag{7}$$

Note that the Green's functions obey reciprocity between source and geophones, namely that $G(\underset{\sim}{x}',\underset{\sim}{x}) = G(\underset{\sim}{x},\underset{\sim}{x}')$. Fourier transforming over the source location x_s and geophone location x_g yields

$$\delta \tilde{u}(k_s, k_g) = \int_V k^2 \delta W(\underset{\sim}{x}) \tilde{G}(k_s,\underset{\sim}{x}) \tilde{f}(k_s) \tilde{G}(k_g,\underset{\sim}{x}) d\underset{\sim}{x} \quad . \tag{8}$$

So far the development assumed nothing about the Green's functions and hence nothing about the background medium $W_0(\underset{\sim}{x})$. Now, I will assume the simplest inhomogeneous non-smooth background medium, namely the previously mentioned two-halfspace model. Furthermore, I will assume the anomaly region is above the interface and below the

source/geophone surface (see Figure 1). In that case, the approximate Green's functions for the background medium above the halfspace-halfspace interface are

$$\tilde{G}(k_s,\underset{\sim}{r}) = \tilde{G}^{+}(k_s,\underset{\sim}{r}) + \tilde{G}^{-}(k_s,\underset{\sim}{r})$$

$$= \frac{i}{2}\frac{\exp(i\gamma_s d_s^{+})}{\gamma_s}\exp(-ik\underset{\sim}{\hat{s}}^{+}\cdot\underset{\sim}{r}) + \tilde{c}(k_s)\frac{i}{2}\frac{\exp(i\gamma_s d_s^{-})}{\gamma_s}\exp(-ik\underset{\sim}{\hat{s}}^{-}\cdot\underset{\sim}{r}) \quad , \qquad (9a)$$

and

$$\tilde{G}(k_g,\underset{\sim}{r}) = \tilde{G}^{+}(k_g,\underset{\sim}{r}) + \tilde{G}^{-}(k_g,\underset{\sim}{r})$$

$$= \tilde{c}(k_g)\frac{i}{2}\frac{\exp(i\gamma_g d_g^{+})}{\gamma_g}\exp(-ik\underset{\sim}{\hat{g}}^{+}\cdot\underset{\sim}{r}) + \frac{i}{2}\frac{\exp(i\gamma_g d_g^{-})}{\gamma_g}\exp(-ik\underset{\sim}{\hat{g}}^{-}\cdot\underset{\sim}{r}) \quad , \qquad (9b)$$

where $\underset{\sim}{\hat{s}}$ and $\underset{\sim}{\hat{g}}$ are the unit vectors pointing along the direction of wave propagation away from the origin towards the source and geophone locations locations respectively and d_s and d_g are the vertical distances between the origin and the source/geophone surface. Note that the first term in equation (9a) and the second term in equation (9b) are the same as the Green's functions given by Wu and Toksöz (1987) for a homogeneous medium while the other terms correspond to reflected waves generated by the halfspace-halfspace interface.

The superscripts on the Green's functions indicate whether the waves are downgoing (+) or upgoing (−) at the origin. The vertical distances traveled by the waves corresponding to each Green's function are denoted d. For instance, d_s^{+} is the vertical distance from the source to the origin (i.e. the anomaly depth) and d_s^{-} is the vertical distance from source down to the interface and back up to the origin (i.e. the vertical distance traveled by a wave that propagates from the source down to the deep interface to be reflected back up to the anomaly). Specifically, from Figure 1, $d_s^{+} = z_0$, $d_s^{-} = 2z_1 - z_0$, $d_g^{+} = 2z_1 - z_0$, and $d_g^{-} = z_0$. Similarly, $\underset{\sim}{\hat{s}}^{+}$ is the unit vector that points toward the source along a ray that travels in the positive depth direction (downward) while $\underset{\sim}{\hat{s}}^{-}$ is the unit vector that points toward the source along a ray that travels in the negative depth direction (upward). Thus, the $\underset{\sim}{\hat{s}}^{-}$ corresponds to the source end of the S^{-+} or S^{--} raypaths shown in Figure 2. Likewise, $\underset{\sim}{\hat{g}}^{+}$ and $\underset{\sim}{\hat{g}}^{-}$ are unit vectors pointing along the two raypaths between the geophones and the origin. The vertical wavenumbers denoted γ_s and γ_g are specified by

$$\gamma_s = \sqrt{k^2 - k_s^2} \quad , \qquad (10a)$$

and

$$\gamma_g = \sqrt{k^2 - k_g^2} \quad , \qquad (10b)$$

and $\tilde{c}(k')$ is the reflection coefficient of the halfspace-halfspace interface for an angle of incidence corresponding to wavenumber k and horizontal wavenumber k' (denoting the source k_s or geophone wavenumber k_g). Notice that waves can travel from the source to the anomaly and then either go up to the geophones or go down to the reflector to be reflected back up to the geophones. These two alternate paths from the anomaly to the geophones

are included as two terms in the geophone Green's function $G(k_g,\underset{\sim}{x})$. Similarly, the source Green's function $G(k_s,\underset{\sim}{x})$ describing how waves can get from the source to the anomaly has two components.

Recall that equation (8) is a first order Born approximation so reverberations in the anomalous region have been excluded. Furthermore, the Green's functions of equation (9) are also approximate to first order because they assume that the sources and geophones are located along an absorbing Earth's surface whereas the real Earth's surface is better approximated as a free surface which would generate multiple reflections of second order. Neither of these approximations detract from the following analysis which shows that first order tomographic terms as well as fisrt order migration terms are included in inversion provided the background model generates reflections.

Substituting the approximate Green's functions into equation (8) yields the equation for the perturbations of the field variable in terms of the squared slowness anomaly

$$\delta\tilde{u}(k_g,k_s) \;=$$

$$-\frac{\tilde{f}(k_s)k^2}{4\gamma_s\gamma_g}\left\{\begin{array}{c}\exp(i\gamma_s d_s^+ + i\gamma_g d_g^-)\int_V \delta W(\underset{\sim}{x})\exp[-ik(\hat{\underset{\sim}{s}}^+ + \hat{\underset{\sim}{g}}^-)\cdot\underset{\sim}{x}]d\underset{\sim}{x} \\ +\tilde{c}(k_g)\tilde{c}(k_s)\exp(i\gamma_s d_s^- + i\gamma_g d_g^+)\int_V \delta W(\underset{\sim}{x})\exp[-ik(\hat{\underset{\sim}{s}}^- + \hat{\underset{\sim}{g}}^+)\cdot\underset{\sim}{x}]d\underset{\sim}{x} \\ +\;\tilde{c}(k_g)\exp(i\gamma_s d_s^+ + i\gamma_g d_g^+)\int_V \delta W(\underset{\sim}{x})\exp[-ik(\hat{\underset{\sim}{s}}^+ + \hat{\underset{\sim}{g}}^+)\cdot\underset{\sim}{x}]d\underset{\sim}{x} \\ +\;\tilde{c}(k_s)\exp(i\gamma_s d_s^- + i\gamma_g d_g^-)\int_V \delta W(\underset{\sim}{x})\exp[-ik(\hat{\underset{\sim}{s}}^- + \hat{\underset{\sim}{g}}^-)\cdot\underset{\sim}{x}]d\underset{\sim}{x}\end{array}\right\}$$

$$= S^{+-} + S^{-+} + S^{++} + S^{--} \quad . \tag{11}$$

Note that there are four scattering terms in this expression are denoted respectively S^{+-}, S^{-+}, S^{++} and S^{--}. Figure 2 shows the corresponding raypaths and illustrates the meaning of the superscripts.

The first two terms are the reflection scattering terms. It is these that lead to the resolution of high vertical wavenumbers in the inversion formulas for squared slowness.

In a homogeneous background there would only be one term, the S^{+-} term (e.g. Wu and Toksöz, 1987). This term corresponds to waves that travel down from the source and are scattered by the velocity anomaly back up to the geophones. Therefore, it represents scattering from waves incident from above. Notice that the presence of the deeper reflector has introduced three other terms.

The S^{-+} term corresponds to waves that travel down from the source, reflect up from the halfspace-halfspace interface, are downward scattered (reflected) from the anomaly back to the interface and are then reflected back up to the geophones.

The last two terms are the transmission scattering terms. It is these that lead to the resolution of the low vertical wavenumbers in the inversion formulas for squared slowness.

The S^{++} term corresponds to waves that travel down from the source, are downward scattered (transmitted) through the anomaly to the interface and then reflected back up to the geophones.

Similarly, the S^{--} term corresponds to waves that travel down from the source, are reflected back up from the halfspace-halfspace interface and subsequently upward scattered (transmitted) through the anomaly to the geophones.

In other words, the S^{+-} and S^{-+} terms will lead to migration-like terms in the inversion formulas while the S^{++} and S^{--} terms will lead to reflection tomography-like terms (c.f. Devaney, 1984). S^{+-} yields the usual migration term, S^{-+} corresponds to back-scattering of waves incident upon the anomaly from below due to deeper reflectors so it yields an underside imaging term, and S^{++} and S^{--} correspond to transmission scattering and thus yield tomographic terms. Mora (1987c) pointed out the corresponding four terms for the case of elastic inversion and suggested how to use these terms to simultaneously resolve both the high and low wavenumbers in the velocity model.

Earlier, I said I would base my development and conclusions on first order effects. Hence, strictly speaking, I am restricted to distributions in the Earth where velocity perturbations are relatively small ($\delta v/v << 1$) such that the back-scattering or reflection coefficients are small and the forward-scattering or transmission coefficients are close to unity. In this context, it is clear that the underside scattering term S^{-+} of equation (11) must also be of second order because it represents a double back-scattering. Therefore, to first order, equation (11) becomes

$$\delta\tilde{u}(k_s, k_g) = S^{+-} + S^{++} + S^{--} \quad .$$

In the following development of the inverse formulas, I will continue to carry the second order S^{-+} term for completeness although no conclusions will be drawn from any terms that result from its presence.

Equation (11) can be written as

$$\delta\tilde{u}(k_s, k_g) = -\frac{\tilde{f}(k_s)k^2 C(\hat{\underset{\sim}{s}})C(-\hat{\underset{\sim}{g}})}{4\gamma_s\gamma_g}\exp[i\gamma_s D_s(\hat{\underset{\sim}{s}}) + i\gamma_g D_g(\hat{\underset{\sim}{g}})] \times$$

$$\int_V \delta W(\underset{\sim}{x})\exp[-ik(\hat{\underset{\sim}{s}} + \hat{\underset{\sim}{g}})\cdot\underset{\sim}{x}]d\underset{\sim}{x} \quad . \tag{12}$$

Now there appears to be only one term because $\hat{\underset{\sim}{s}}$ and $\hat{\underset{\sim}{g}}$ span 360 degrees while previously the $\hat{\underset{\sim}{s}}^+$, $\hat{\underset{\sim}{s}}^-$, $\hat{\underset{\sim}{g}}^+$ and $\hat{\underset{\sim}{g}}^-$ vectors only spanned 180 degrees each. For convenience, I have lumped together reflection coefficient terms like $\tilde{c}(k')$ into $C(\hat{\underset{\sim}{s}})$ and $C(-\hat{\underset{\sim}{g}})$. Similarly, d_s^+ and d_s^- were included in D_s and d_g^+ and d_g^- in D_g. For example,

$$D(\hat{\underset{\sim}{s}}) = \begin{cases} d_s^+ & \textit{when } \hat{\underset{\sim}{s}} \textit{ corresponds to a downgoing ray} \\ d_s^- & \textit{when } \hat{\underset{\sim}{s}} \textit{ corresponds to an upgoing ray} \end{cases} .$$

Therefore, equation (12) can be considered to be a generic term of equation (11). Three dimensional Fourier transformation of equation (12) yields the generic equation for the squared slowness anomaly in terms of the perturbation in the wavefield

$$\delta\tilde{W}[k(\hat{\underset{\sim}{g}}+\hat{\underset{\sim}{s}})] = -\delta\tilde{u}(k_s,k_g)\,\frac{4\gamma_s\gamma_g}{\tilde{f}(k_s)k^2C(\hat{\underset{\sim}{s}})C(-\hat{\underset{\sim}{g}})}\exp\left\{-i[\gamma_s D_s(\hat{\underset{\sim}{s}})+\gamma_g D_g(\hat{\underset{\sim}{g}})]\right\} \quad . \quad (13)$$

Note that I assumed that $C(\hat{\underset{\sim}{e}}) \neq 0$ for all directions $\hat{\underset{\sim}{e}}$ and $\tilde{f}(k_s) \neq 0$ (i.e. the reflection coefficient and source strength are both non-zero for all wavenumbers). Normally, one would apply a small damping term to the denominator to stabilize the solution. Hence, zero's in the source or reflection coefficient at a given wavenumber would result in holes in the wavenumber spectrum for squared slowness.

THE RESOLVED WAVENUMBER SPECTRUM

Equation (13) relates one plane wave component in the wavenumber spectrum in squared slowness to the wavenumbers of the acoustic waves along the source and geophone axes. Consider the single frequency experiment where the frequency of the source ω is fixed so the length of the vectors $k\hat{\underset{\sim}{s}}$ and $k\hat{\underset{\sim}{g}}$ are constant. Now both $\hat{\underset{\sim}{s}}$ and $\hat{\underset{\sim}{g}}$ span 360 degrees thanks to the reflecting interface between the two halfspaces (if the interface were not present then we would only have the S^{+-} term and $\hat{\underset{\sim}{s}}$ and $\hat{\underset{\sim}{g}}$ would only span 180 degrees). If we fix $\hat{\underset{\sim}{s}}$ and let $\hat{\underset{\sim}{g}}$ span 360 degrees then a circular zone will be resolved in the wavenumber spectrum of the squared slowness (Figure 3). Now, by letting the source vector $\hat{\underset{\sim}{s}}$ range from 0 to 360 degrees, the entire wavenumber spectrum of the squared slowness will be resolved up to some maximum depending on the frequency ω (Figure 4). Consequently, when sources and geophones are located on the Earth's surface, a single frequency seismic source will resolve the *entire* wavenumber spectrum of the squared slowness up to a maximum value of $2\omega/v_0$.

To see in detail how the entire squared slowness spectrum is resolved and how the non-constant background relates to the constant background case, I will divide the spectrum into four components. These are derived from the four terms of equation (11). Thus, equation (13) can be written as the sum of four inversion terms

$$\delta\tilde{W}[k(\hat{\underset{\sim}{s}}+\hat{\underset{\sim}{g}})] = I^{+-} + I^{-+} + I^{++} + I^{--}$$

$$= -\delta\tilde{u}(k_s,k_g)\,\frac{4\gamma_s\gamma_g}{\tilde{f}(k_s)k^2}\begin{pmatrix} \exp[-i(\gamma_s d_s^+ + \gamma_g d_g^-)] \\ + \frac{1}{\tilde{c}(k_g)\tilde{c}(k_s)}\exp[-i(\gamma_s d_s^- + \gamma_g d_g^+)] \\ + \frac{1}{\tilde{c}(k_g)}\exp[-i(\gamma_s d_s^+ + \gamma_g d_g^+)] \\ + \frac{1}{\tilde{c}(k_s)}\exp[-i(\gamma_s d_s^- + \gamma_g d_g^-)] \end{pmatrix}$$

$$= -\frac{\delta\tilde{u}(k_s,k_g)}{\tilde{f}(k_s)k^2}\left(\frac{4\gamma_s\gamma_g}{C(\underset{\sim}{\hat{s}})C(-\underset{\sim}{\hat{g}})}\right)^2 \tilde{G}^*(k_s,k(\underset{\sim}{\hat{s}}+\underset{\sim}{\hat{g}}))\tilde{G}^*(k_g,k(\underset{\sim}{\hat{s}}+\underset{\sim}{\hat{g}})) \quad , \qquad (14)$$

where the asterisk indicates conjugate transpose. The division by $\tilde{f}(k_s)$ is deconvolution to remove the source signature and the division of some terms by reflection coefficients allows for the strength of the deeper reflection. As in equation (11), the vectors $\underset{\sim}{\hat{s}}^+$, $\underset{\sim}{\hat{s}}^-$, $\underset{\sim}{\hat{g}}^+$ and $\underset{\sim}{\hat{g}}^-$ span 180 degrees each. The first term, the I^{+-} term is the usual homogeneous background term. The part of the squared slowness spectrum resolved by this term is shown in Figure 5 (a). It was evaluated at a single frequency ω by letting the vectors $\underset{\sim}{\hat{s}}^+$ and $\underset{\sim}{\hat{g}}^-$ span through the appropriate 180 degree ranges (c.f. Figure 4 where $\underset{\sim}{\hat{s}}$ and $\underset{\sim}{\hat{g}}$ both spanned 360 degrees) and using symmetry to fill in the wavenumber spectrum for $k_z < 0$ (i.e. I assume that the velocities are real so the wavenumber spectrum has 2D conjugate symmetry). Similarly, the spectra resolved by the other three terms are also shown in Figure 5. It is clear that the usual homogeneous background term (the I^{+-} term) leaves big holes in the spectrum, particularly in the low vertical wavenumbers. The three extra inhomogeneous background terms fill the rest of the spectrum. In particular, the I^{++} and I^{--} terms fill in the low vertical wavenumbers. Furthermore, the I^{+-} term is the inverse reflection scattering term for waves incident from above while the I^{-+} term is the inverse reflection scattering term for reflected waves incident from below. Similarly, the I^{++} term is the inverse transmission scattering term for waves incident from above while the I^{--} term is the inverse transmission scattering term for waves incident from below (see Figure 2 for a ray diagram of the corresponding four scattering terms). Note that I^{+-} and I^{-+} resolve the same part of the wavenumber spectrum. Two holes are in this spectrum in exactly in the place where I^{++} and I^{--} are resolved. Figure 5 illustrates the complimentary nature of the I^{+-} and I^{-+} migration-like terms with the I^{++} and I^{--} reflection tomography terms.

Observe that the I^{-+} term derived from the second order S^{-+} scattering term so no first order conclusions can be drawn from the presence of this term. If this term *was* included in an inversion of noisy data, the reliability of the solution would decrease by a factor of order $O(\delta u, \delta W)$. I will continue to reference $(-+)$ terms for completeness although no practical significance should be attached to such terms.

THE TOMOGRAPHIC TERMS REVEALED

To illustrate the migration and tomographic inversion terms when the reflector depth is known, consider an inversion of the synthetic data shown in Figure 6. It was generated by modeling through a background consisting of a circular velocity anomaly embedded in the upper halfspace of a two-halfspace model (Figure 7 (a)). The source wavelet was missing both high and low frequencies being a fourth derivative of a Gaussian curve. An iterative

inversion to solve for the velocities was carried out (i.e. equation (14) was evaluated). The initial model used in the inversion was the two-halfspace model. This model was identical with the model that was used to generate the synthetic data except that the circular anomaly was missing from the upper halfspace. The inversion result (Figure 7 (b)) contains the circular anomaly and two weak V shaped features roughly emanating from the source location at zero km and passing through the velocity anomaly. These V's are the contributions from the tomographic terms I^{++} and I^{--} and look like the ray trajectories for the transmission scattering terms S^{++} and S^{--} shown in Figure 2. The migration terms I^{+-} and I^{-+} have sharpened the outline of the circle and slightly repositioned the deeper reflector. The repositioning is seen as a flat event in the inversion result shown in Figure 7 (b). If many shot gathers were used in the inversion, the velocity anomaly would have been illuminated from many different directions (just like the human body in medical imaging). Hence a more complete picture (without V's) would be obtained as will be seen in the following example. Only one shot gather was used in this inversion to illustrate the effects of the different inversion terms. Also, the reflector depth was supplied (i.e. the initial inhomogeneous background velocity consisted of the true two halfspace model). The following examples demonstrate that iterative inversions do not require knowledge of reflector depth.

RELATIONSHIP TO ITERATIVE INVERSION

To illustrate the concept of obtaining both high and low wavenumbers simultaneously *without* prior knowledge of an inhomogeneous background model, I will use the algorithm derived by Tarantola (1984) and extended and tested by Mora (1987a,1987b). This method performs an elastic inversion by conjugate gradient iterations. I will restrict the calculations to the constant density acoustic case (shear velocities equal to zero and density fixed) in order to simplify the interpretation of the results. The algorithm is based on the elastic wave equation. It attempts to match an observed wavefield with a synthetic wavefield generated by modeling through some velocity model. When the match between the two wavefields is good then the algorithm has converged to the most probable velocity model under the assumptions of least squares (i.e. Gaussian errors in the data and Gaussian distributed velocities). From Mora (1987a), the P-wave velocity perturbation at the $(n+1)$-th iteration $\delta v^{n+1}(\underset{\sim}{\mathrm{r}})$ in terms of the data perturbation at the n-th iteration $\delta u^n(x_g,t) = u_0^n(x_g,t) - u_{obs}(x_g,t)$ is

$$\delta v^{n+1}(\underset{\sim}{\mathrm{r}}) \propto \sum_s \int dt\, [\sqrt{t}G^n(x_s,\underset{\sim}{\mathrm{r}},t) * f(x_s,t)][\sum_g \sqrt{t}G^n(x_g,\underset{\sim}{\mathrm{r}},-t) * \delta u^n(x_s,x_g,t)] + \varepsilon\,, \tag{15}$$

where $u_{obs}(x_g,t)$ is the observed seismic data and $*$ denotes convolution over time and $u(\underset{\sim}{\mathrm{r}}) = \nabla\cdot\mathbf{U}(\underset{\sim}{\mathrm{r}})$ where $\mathbf{U}(\underset{\sim}{\mathrm{r}})$ is the displacement vector. Equation (15) is applied iteratively in a conjugate gradient algorithm until the data perturbation is zero. At this point, synthetic data generated from the velocity model matches the observed data $u_{obs}(x_g,t)$. For small

velocity perturbations and no damping, the iterative time-space domain expression given by equation (15) yields exactly the same solution as the frequency-wavenumber domain expression given by equation (14). This is easily seen by integrating equation (14) over the data space (sources, geophones and frequency) and inverse transforming to the time-space domain

$$\delta W(\underset{\sim}{x}) \propto \sum_s \sum_g \left[\hat{G}(x_s,\underset{\sim}{x},-t) * f^{-1}(x_s,t) * \hat{G}(x_g,\underset{\sim}{x},-t) * \delta u(x_s,x_g,t)\right]_{t=0}$$

$$= \sum_s \int dt[\hat{G}(x_s,\underset{\sim}{x},t) * f^{-1}(x_s,t)][\sum_g \hat{G}(x_g,\underset{\sim}{x},-t) * \delta u(x_s,x_g,t)] \quad , \qquad (16a)$$

where

$$\hat{G} = \frac{G}{|G|} \sim \frac{\sqrt{t}\, cos(\theta) G}{C} \quad , \qquad (16b)$$

is a normalized Green's function in two dimensions and θ is the angle of wave propagation. It is clear that, when restricted to the acoustic case, the equations of Mora (1987a) given by equation (15) are the essentially the same as the inversion formulas of this paper given in equation (16). Differences are:

(i) the Green's functions have been scaled differently because $\sqrt{t}$ = *divergence correction* $\neq$ $1/|G|$ except if incidence angles are small (i.e. $cos(\theta) \approx 1$) and the velocity model is homogeneous (i.e. has no reflectors) so C is unity,

(ii) there is a convolution in equation (15) with the source wavelet whereas there is a deconvolution with the source wavelet in equation (16),

(iii) equation (15) has a damping term and is applied iteratively.

The conjugate gradient iterations ensure that the synthetic data matches the observed data and hence corrects (though perhaps inefficiently) for all of these differences. To speed the convergence of the iterations, one could easily enough deconvolve rather than convolve with the source wavelet and rescale the Green's functions. In particular, one could allow for the reflection strength by dividing equation (15) by the C factor as was done in equation (16). Mora (1987c) described this concept and in particular observed that

$$\delta v^{n+1} = [J^{+-} + J^{-+}] + [J^{++} + J^{--}] + \varepsilon \sim [I^{+-} + \bar{C}^2 I^{-+}] + \bar{C}[I^{++} + I^{--}] + \varepsilon$$

$$= [migration - like\ terms] + [reflection - tomographic - like\ terms] + [damping\ term] \quad . \qquad (17)$$

leading to the conclusion that the convergence could be sped up by boosting the reflection-tomographic terms (i.e. J^{++} and J^{--}). Clearly, the boost factor should be about equal to the inverse of the reflection coefficient at a representative angle of incidence denoted $\bar{C}$. Specifically, use in the iterative formula

$$\delta v^{n+1} = [J^{+-} + \frac{1}{\bar{C}^2} J^{-+}] + \frac{1}{\bar{C}}[J^{++} + J^{--}] + \varepsilon \approx 2J^{+-} + \frac{1}{\bar{C}}[J^{++} + J^{--}] + \varepsilon \quad , \qquad (18)$$

where I assumed that $J^{-+} \approx J^{+-}$ because J^{-+} supplies about the same information as J^{+-} (Figure 5). Note that the reflector in the following example is strong (i.e. $\bar{C} \approx 1$) so it was not necessary to boost the tomographic terms to achieve rapid convergence. Recall that the J^{+-}, J^{++} and J^{--} inversion terms all derive from first order scattering effects and thus have the same reliability.

EXAMPLES WHEN REFLECTOR DEPTHS ARE NOT KNOWN

Iterative inversion without deeper reflectors

Both of the following examples used a fourth derivative of a Gaussian curve as the source wavelet. This is a narrow-band wavelet that is missing both low and high frequencies. Therefore, there can be no questions as to whether low wavenumbers present in the inversion solutions are due to low frequencies in the source (i.e. low wavenumbers in the inversion solution cannot be attributed to the presence of low frequencies in the source wavelet because there were none).

Figure 8 shows one of the five shot gathers used in the inversion which was generated by finite difference modeling over a circular anomaly embedded in a homogeneous halfspace (Figure 9 (a)). There is *no* deep reflector (i.e. $\bar{C} = 0$ in equation (17)) so that the inversion formula given by equation (15) implicitly contains only the usual migration-like term (the I^{+-} term). An inversion was performed using a homogeneous starting model. Figures 9 (b) and 9 (c) shows the inversion result after one and fifteen iterations. The mismatch after fifteen iterations was small (about 12%) so the algorithm has largely, though not completely, converged. The fifteen-iteration result contains only high wavenumbers and looks very similar to a migration result (the first-iteration result). This is because the background model was homogeneous and there were no deeper reflectors.

Iterative inversion with deeper reflectors

Now consider the same model but with a strong deeper reflector. The starting model was again homogeneous so the reflector location was *not* assumed to be known a priori. The deep reflector is strong so no boosting of the reflection-tomographic terms was necessary (see the description of boosting after equation (17)). One of the five shot gathers used in the inversion is shown in Figure 10. The true model and the one- and fifteen-iteration inversion results are in Figure 11. The first-iteration result is the same as in the previous example except that the deeper reflector has been imaged. However, after fifteen iterations, the circular anomaly region, particularly its interval velocity, is better reconstructed and contains both high and low wavenumbers (i.e. both its boundaries and its interval velocity

have been found). In other words, the interval velocity inside the circular region is now almost constant and the circular anomaly located by the inversion has almost exactly the same appearance as the true circular anomaly of Figure 11 (a). By comparison, the result shown in Figure 9 (c) looked like a high pass filtered version of the true anomaly. One reason the anomaly is not more perfectly reconstructed by the inversion is that fifteen iterations were not adequate for the conjugate gradient algorithm to completely converge. Also, there are small smear artifacts due to the finite number of geophones (101 along the Earth's surface) and sources (five located every 0.5 km starting from 0.0 km).

Discussion of inversion results when the reflector depths were unknown

The initial model used in both the above examples was constant and had a velocity equal to that of the upper halfspace in the true model. Therefore, the first iteration of the inversion was essentially a migration and located approximately the reflectors (see Mora (1987a) for a discussion of why the first iteration of an inversion is similar to a migration). The first example had no deeper reflectors so the extra tomographic terms did not come into play and only the high wavenumbers could be resolved.

However, the second example had a deeper reflector. Once it was approximately located by the first iteration, the three extra terms (one migration and two reflection tomographic terms) discussed earlier had an effect in the inversion. These helped better reconstruct: (i) the underside of the circular region (the I^{-+} term of equation (14) which is significant in this example because $\bar{C} \approx 1$) and, (ii) the interval velocity (the I^{++} and I^{--} terms of equation (14)). Subsequent iterations adjusted the velocity model in order to best match the wavefield computed from this model to the "observed" wavefield. Both the reflector location and the interval velocity model were adjusted simultaneously as the iterations proceeded.

DISCUSSION

Iterative inversion

I have shown that low vertical wavenumbers in velocity are recovered in an inversion when the background velocity contains sharp discontinuities. The examples illustrate that iterative inversion that updates the velocity model can obtain both high and low wavenumbers in the velocity model. At least two iterations are necessary to solve for the velocities if a smooth velocity model is used as the starting guess (i.e. no a priori knowledge of reflector locations is assumed). The first iteration will approximately locate the reflectors and the second will solve for the interval velocities. Only two iterations are required provided (i) the problem is linear (i.e. there are small velocity perturbations, infinite offsets and Gaussian

noise), and (ii) a Newton algorithm rather than a conjugate gradient algorithm is used (i.e. $1/|G|$ is applied). Typically, velocity perturbations are not so small and offsets are finite so the inverse problem is nonlinear. Consequently, more than two iterations are usually required to obtain the complete solution even with a Newton algorithm. Actually, it is often more efficient to use a conjugate gradient method and iterate rather than a Newton method when the velocity model is complex. This is because the inverse Hessian (or equivalently $1/|G|$) required by Newton algorithm's is typically very expensive to compute in comparison to some conjugate gradient iterations. Future research will be required to investigate the utility of the low-wavenumber reflection tomographic terms in the inversion formulas when gradient based inversion schemes are used. This is especially true when many reflectors are present because the boosting factor $(1/\bar{C})$ required by the tomographic terms becomes spatially variable.

Resolution of reflector location and interval velocity

The first iteration essentially does a depth migration and therefore approximately locates the reflectors. If the velocity model is not quite correct, the positioning of reflectors is slightly incorrect. One may ask whether this would unduly affect the inversion. Does the analysis in this paper remain valid considering I assumed that the reflector location was known? Would mispositioning of reflectors affect the ability of the algorithm to resolve the low wavenumbers? The quick answer is "no" provided there are enough offsets to remove (or partially remove) ambiguities between the reflector positions and interval-velocities.

Considering the position of the reflectors is influenced by the initial low-wavenumber velocity model, there is certainly some interaction between the low and high wavenumbers. Consider a single source and single geophone experiment. In that case, it is impossible to resolve between the depth of a reflector and the interval velocity down to that reflector (i.e. if traveltime $t = z/v$ is observed then we cannot differentiate between an increase in velocity v and a decrease in depth z). However, when several sources and geophones are used, the shapes of the reflection events helps distinguish interval velocity from reflector depth. Also, as the number of illumination angles of waves passing through the upper halfspace are increased, the resolution between depth and velocity increases. This is why the example with five sources and 101 geophones converged to a good solution even though the reflector depth was not specified. Hence, I conclude that while the low and high wavenumbers do interact as the iterations proceed, they can be resolved from one another if enough conjugate gradient iterations are performed. The iterations slowly reposition the reflector(s) and update the interval velocities until the solution is obtained (see Figure 9 (c)).

Local minima

One further difficulty with inversion schemes is that they may converge to local minima (on the square error functional that measures the mismatch between observed and synthetic

data). This is avoided by starting with a velocity model that is sufficiently close to the solution. In my experience with seismic inversion, sufficiently close means the initial velocity model must describe the kinematics of wave propagation to within about a half a fundamental wavelength of the seismic source wavelet. In order to obtain this starting velocity model, an initial inversion step (perhaps interpretive, such as velocity analysis) may still be required.

The likelihood of a local minima is lessened when doing iterative inversion that vary the high- and low-wavenumber velocity model. This is because the velocity model can converge on the low wavenumbers from the top of the model down as the iterations proceed. Thus, throughout the iterations there will always be an "uppermost portion of the model" that obeys the half a wavelength criterion. Consequently, provided the iterations are not too expensive, it may not even be necessary to do the velocity analysis in order to do a complete inversion for all wavenumbers. Alternatively, Mora (1987a) suggested how to redefine the objective function to be sensitive to the low wavenumbers and perhaps less nonlinear.

Incomplete data

In this paper, I derive and plot the wavenumber spectra of velocity perturbations that can be resolved from a single frequency seismic source when offset ranges are infinite. I showed that all wavenumbers could be resolved up to some maximum value, namely, double of the frequency of the seismic source (see Figures 3 and 4).

In real experiments where seismic sources are band-limited and offsets are restricted to some finite range, some parts of the wavenumber spectrum simply cannot be resolved using surface seismic data. Figure 12 shows the part of the wavenumber spectrum that can be resolved from such incomplete (and more realistic) data. Figure 12 was obtained by the same procedure that was used to generate Figure 3 by letting $\hat{\underset{\sim}{s}}^+$, $\hat{\underset{\sim}{s}}^-$, $\hat{\underset{\sim}{g}}^+$ and $\hat{\underset{\sim}{g}}^-$ span an angle less than 180 degrees (to allow for a finite offset range) and with sources ranging over a "band" of frequencies.

Of course, in real surveys where sources and geophones must be at discrete locations, the resolved wavenumber spectrum is also discrete.

CONCLUSIONS

It is crucial in inversion and diffraction tomography of surface seismic data to use an inhomogeneous background velocity in order to resolve the entire wavenumber spectrum of the velocity model. Iterative inversion that varies the background velocity model (both high- and low-wavenumber components) *can* find *all* wavenumbers in the velocity spectrum except those that cannot be resolved due to incompleteness of the data set (e.g. finite offset ranges etc).

These kinds of inversion are like a combination of iterative migration and reflection tomography. The high wavenumbers (the reflector model) are obtained by migration terms and the low wavenumbers (the upper halfspace interval velocities) are found by diffraction tomography terms. Both the reflector model and the interval velocities are obtained simultaneously and automatically in iterative wave equation inversion schemes.

Because the low wavenumbers can be reconstructed in iterative inversion, elastic inversion schemes such as Tarantola (1984) and Mora (1987a) will soon be extendible to perform "complete" inversion of seismic data for all wavenumbers in the spectra of the elastic parameters (see Mora 1987c). On a computer that is capable of sufficiently fast wave simulations such as the CRAY-3 or the 2.5 Gigaflop highly parallel parallel Connection Machine®[1] (Hillis, 1986), these iterative wavefield inversion methods may soon overtake in utility the efficient but partial solutions of velocity analysis and migration.

ACKNOWLEDGEMENTS

I acknowledge the support of the sponsors of the Stanford Exploration Project and Jon Claerbout during this research.

REFERENCES

Devaney, A. J., 1984, Geophysical diffraction tomography: IEEE Trans. Geosci. Remote Sensing, **GE-22** , 3-13.

Devaney, A. J., and Beylkin, G., 1984, Diffraction tomography using arbitrary source-receiver surfaces: Ultrason. Imag., **6**, 181-193.

Esmersoy, C., Oristaglio, M. L., and Levy, C., 1985, Multidimensional Born velocity inversion: Single wide-band point source: J. Acoust. Soc. Amer.,**78**, 1052-1057.

Esmersoy, C., and Levy, C., 1986, Multidimensional Born inversion with a wide-band plane-wave source: IEEE Proc.,**74**, 466-475.

Hillis, W. D., 1986, The connection machine: The MIT Press.

Mora, P., 1987a, Nonlinear 2D elastic inversion of multi-offset seismic data: Geophysics, **52**.

[1]Connection Machine is a registered trademark of Thinking Machines Corporation

Mora, P., 1987b, Elastic wavefield inversion of reflection and transmission data: Geophysics, submitted.

Mora, P., 1987c, Elastic wavefield inversion for low and high wavenumbers of the P- and S-wave velocities, a possible solution: in Proceedings for the research workshop on deconvolution and inversion, September 1986, Rome, Italy.

Tarantola, A., 1984, The seismic reflection inverse problem, in Inverse problems of acoustic and elastic waves, edited by: F. Santosa, Y.H. Pao, W. Symes, and Ch. Holland, SIAM, Philadelphia.

Wu R., and Toksöz, M. N., 1987, Diffraction tomography and multisource holography applied to seismic imaging: Geophysics, **52**, 11-25.

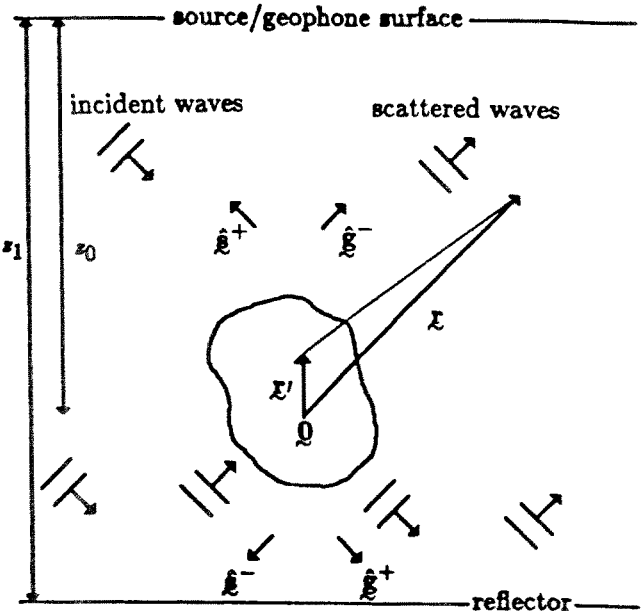

Figure 1: Basic plane wave experiment showing plane waves incident upon a velocity anomaly embedded in a layer over a halfspace.

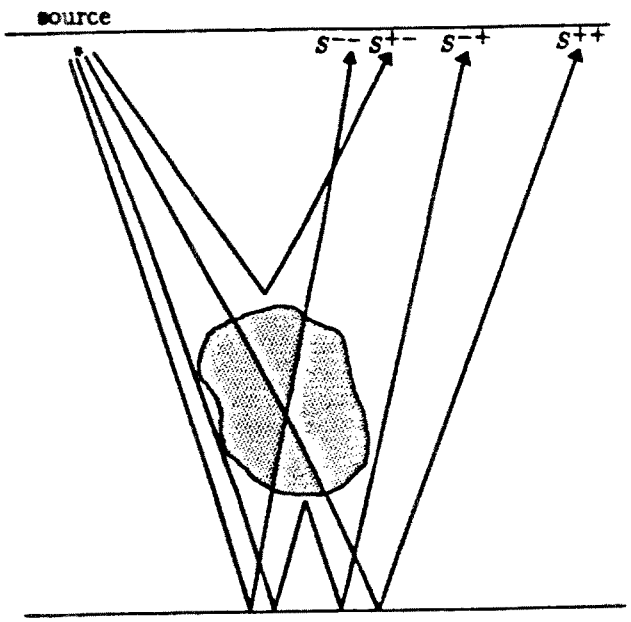

Figure 2: Raypaths corresponding to the four different scattering terms. The first superscript refers to the incident ray direction while the second superscript refers to the scattered ray direction (+ is downward and − is upward). For example, S^{+-} has a downgoing incident ray and an upgoing scattered ray.

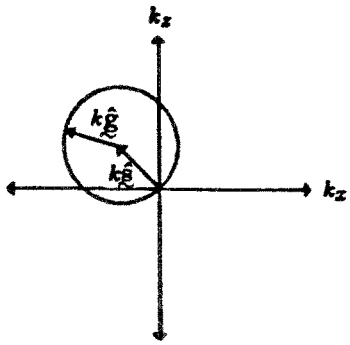

Figure 3: The part of the wavenumber spectrum of the squared slowness model that can be resolved using a single plane wave source.

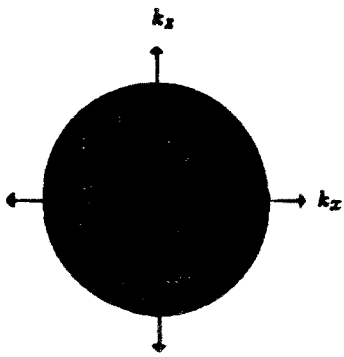

Figure 4: The part of the wavenumber spectrum of the squared slowness that can be resolved using a point source (i.e. a sum of plane waves at all angles).

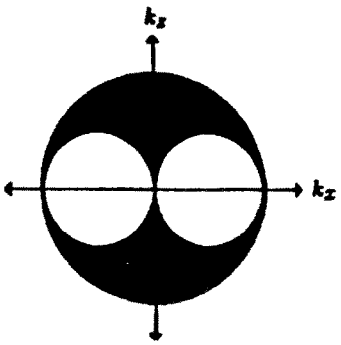

Figure 5: (a) The part of the wavenumber spectrum of squared slowness that can be resolved from the I^{+-} inversion term (i.e. the usual imaging term). This is essentially the same as Wu and Toksöz (1987), Figure 12 (a), except that their spectrum was for a wide-band source rather than a single frequency. This is identical to the part of the wavenumber spectrum of squared slowness that can be resolved from the I^{-+} inversion term (i.e. the underside imaging term).

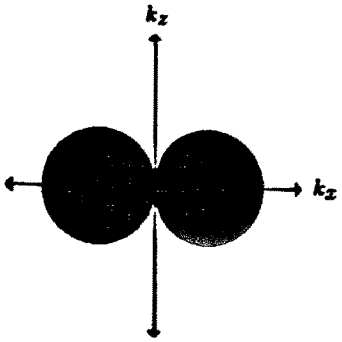

Figure 5: (b) The part of the wavenumber spectrum of squared slowness that can be resolved from the I^{++} inversion term (i.e. the downward path tomographic term). This is identical to the part of the wavenumber spectrum of squared slowness that can be resolved from the I^{--} inversion term (i.e. the upward path tomographic term).

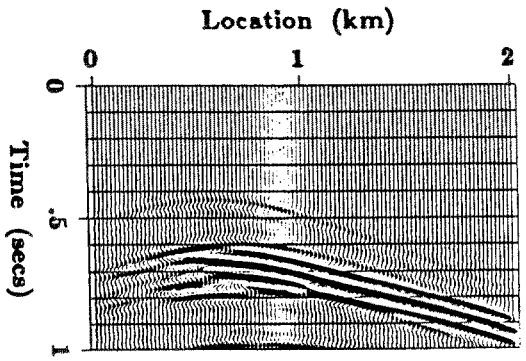

Figure 6: Shot gather generated from the model shown in Figure 7 (a).

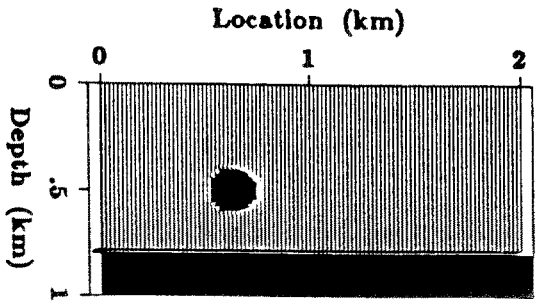

Figure 7: (a) The true model corresponding to the synthetic data shown in Figure 6. Black indicates a negative perturbation and white a positive perturbation relative to the acoustic impedance in the upper layer. The velocity perturbation of the circular region relative to the layer velocity was 10%.

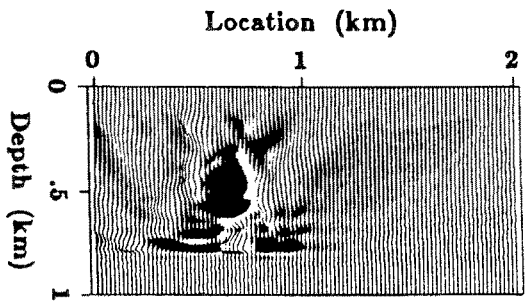

Figure 7: (b) Ten iteration inversion result. The starting model was a layer over a halfspace that was identical to the true model except that that the circular velocity anomaly was not present.

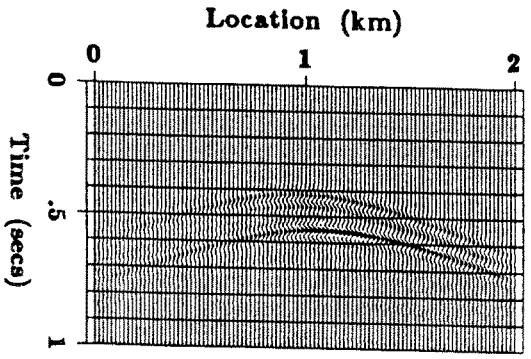

Figure 8: Shot gather generated from the model shown in Figure 9 (a).

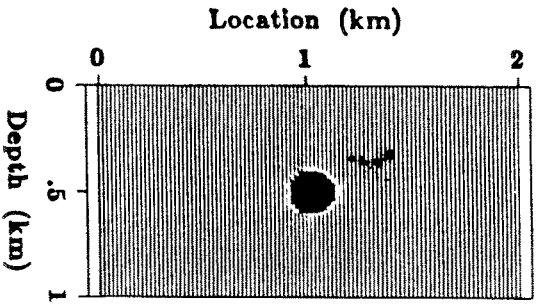

Figure 9: (a) True model corresponding to the synthetic data shown in Figure 8. Black indicates a negative perturbation and white a positive perturbation relative to the acoustic impedance in the upper layer. The velocity perturbation of the circular region relative to the layer velocity was 10%.

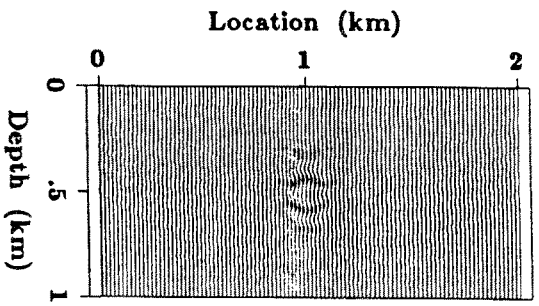

Figure 9: (b) One-iteration inversion result plotted as the perturbation relative to the homogeneous starting model.

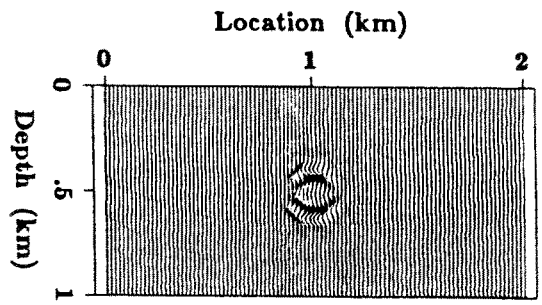

Figure 9: (c) Fifteen-iteration inversion result plotted as the perturbation relative to the homogeneous starting model.

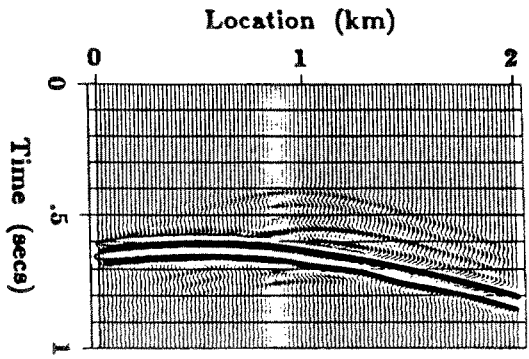

Figure 10: Shot gather generated from the model shown in Figure 11 (a).

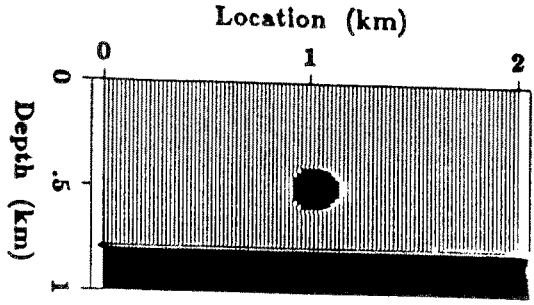

Figure 11: (a) True model corresponding to the synthetic data shown in Figure 10. Black indicates a negative perturbation and white a positive perturbation relative to the velocity in the upper layer. The velocity perturbation of the circular region relative to the layer velocity was 10%.

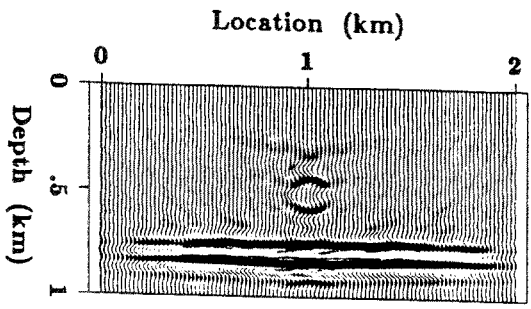

Figure 11: (b) One-iteration inversion result plotted as the perturbation relative to the homogeneous starting model.

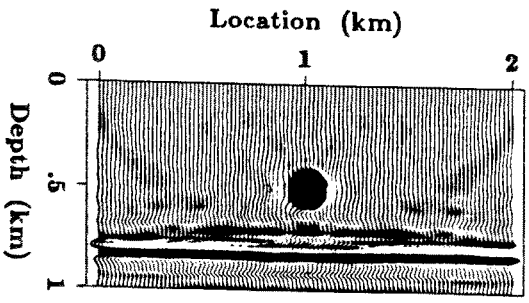

Figure 11: (c) Fifteen-iteration inversion result plotted as the perturbation relative to the homogeneous starting model.

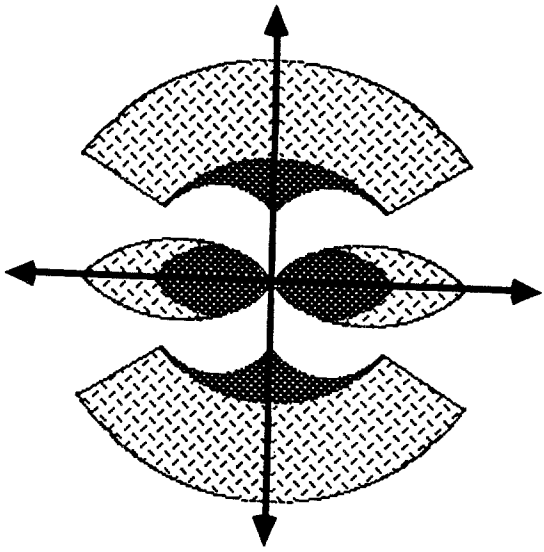

Figure 12: The part of the wavenumber spectrum that can be resolved when the offset range is *finite* and the source is *band-limited*. The dark shaded region is the best resolved part because it receives contributions from by all frequencies in the band. The light shaded region is resolved by progressively less frequencies as one moves further from the darker region.